Engineering Science & Technology
http://ojs.wiserpub.com/index.php/EST/

UNIVERSAL WISER PUBLISHER

Research Article

Influence of Part Size Error on the Characteristics of a Feeding Transmission Mechanisms Based on a Conjugate Cam-Spatial Linkage

Chunwei Zhang[1, 2*], Tao Meng[1], Junqiang Zou[1], Linzheng Zhou[1], Shuwei Li[1]

[1]School of Mechanical Engineering, Yancheng Institure of Technology, Jiangsu, 224051, PR China
[2]Jiangsu Key Laboratory for Design and Manufacture of Micro-Nano Biomedical Instruments, Southeast University, Jiangsu, Nanjing, 210096, PR China
Email: wzhangchun@163.com

Received: 3 November 2022; **Revised:** 16 December 2022; **Accepted:** 19 December 2022

Abstract: Reasonable size accuracy of a mechanical part may be key for the design of the complex transmission mechanism; thus, it is very important to evaluate the size errors of each part. Taking the conjugate cam-spatial rank feeding transmission mechanism as an example, functions such as the near-dwelling, fast-forwarding, working-feeding, slow-forwarding, far-dwelling, fast-returning, quick-feeding-back, and slow-returning are realized with the appropriate conjugate cam governing equations. The analytical expressions of the conjugate cams and the functions of the angular motion and angular velocity between the conjugate cam and crank are derived. Considering the real machining errors of part, a concept of parameter sensitivity is proposed, and the magnitude and direction of the influence of typical parameter errors on the mechanism motion transfer characteristics are evaluated by this concept. This method provides a reliable reference for the precision design of mechanical structure parameters.

***Keywords*:** conjugate cam-spacial linkage, transmission mechanism, machining error, parameter sensitivity

Nomenclature

l_{AO_1}	length of follower arm
l_{OO_1}	distance between cam center O and follower pivot point O_1
r_{base}	base circle radius
l_{qb}	length of auxiliary rod
l_q	length of crank
l_a	length of rocker
α	angular acceleration
β_0	initial angle of crank
β	angle of crank
δ_0	initial angle of rocker
δ	angle of rocker
θ	cam rotation angle

DOI: https://doi.org/10.37256/est.4120232130

θ_{f_fast}	master cam rotation angle for φ_{f_fast}
θ_{f_slow}	master cam rotation angle for φ_{f_slow}
θ_{f_work}	master cam rotation angle for φ_{f_work}
θ_{push}	master cam rotation angle for φ_{max}
θ_{01}	initial mounting angle on the master cam
θ_{02}	initial mounting angle on the complementary cam
φ_{f_fast}	angle of fast-forwarding
φ_{f_work}	angle of working-feeding
φ_{max}	maximum swing angle
φ_{total}	angle between both swing links
φ_{01}	initial angle of swing link on the master cam
φ_{02}	initial angle of swing link on the complementary cam
ω	angular velocity

1. Introduction

The reasonable determination of size error is an important task in mechanical manufacturing and design. The smaller tolerance of part unnecessarily calls for high-precision machining processes, which leads to the increasing difficulty and cost of manufacturing [1]. On the other hand, high tolerance parts make the production unqualified, such as the blade of the aero engine [2]. Therefore, balancing cost and performance is one of the most critical tasks in the design process.

Traditionally, the size tolerance of a part is empirically determined according to its cost and function, such as fit, position, and orientation. However, in the complicated mechanism that contains many parts, as shown in Figure 1, the parts with the so-determined size can often cause incorrect action due to error transfer. Therefore, the tolerance of a part should not be determined individually but in the whole mechanical structure.

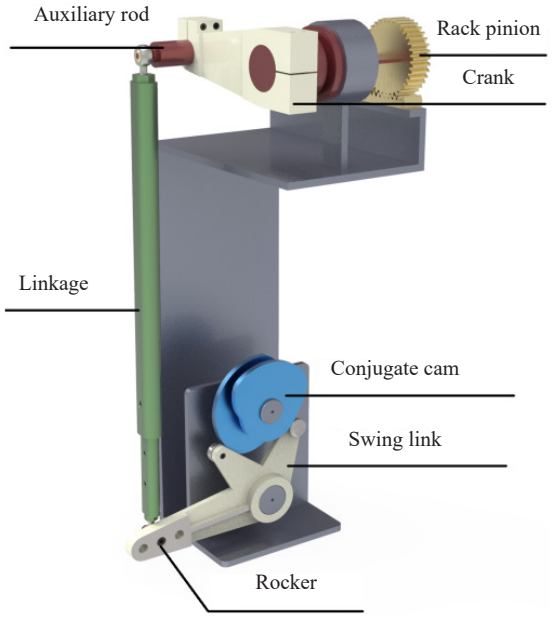

Figure 1. 3D schematic diagram of the conjugate cam-spatial linkage mechanisms

Taking a circular combination machine tool with 12 stations as an example, it is required that the machining time at each station be less than 10 seconds; in other words, a part can be machined every 10 seconds on average. By the analysis of the machining process of the part, it is found that the transfer units are almost the same, only different in parametric sizes, as shown in Figure 1. Each station includes the same motions, such as near-dwelling, fast-forwarding, working-feeding, slow-forwarding, far-dwelling, fast-returning, quick-feeding-back, and slow-returning.

Precise parameters should be provided for constructing the above 3D model in which more than 20 parameters are involved. In practice, parametric errors always exist during the manufacturing and assembly process, such as cam profile errors, subtending angle errors of both the follower linkages [3], linkage length errors, etc. The errors are eventually transferred to the crank, which may result in incorrect motion of the crank.

It is still challenging to determine so many size tolerances because the sizes are correlated. Jiao Yongzhi et al. [4] formulated the error-transferring law of cam-linkage mechanisms by using the complex vector method and found that the same size errors of each component imposed a different influence on the motion law of the printing mechanisms. However, they didn't propose a way to solve the problem. Based on a sensitivity analysis, Mills et al. [5] proposed a method to optimize the parameters, including the cam base-circle radius, follower roller radius, follower offset, cam thickness, return stiffness, and initial compression. Based on the optimization approaches and the reliability analysis, by taking into account the three typical parameters, optimal sizes are obtained, and the corresponding reliabilities are investigated [6].

Many design methods of cam mechanisms have been proposed [7]-[10], but few of them consider how to minimize the motion errors between theory and practice by the precision design of the component. In this paper, to introduce the parameters involved, we initially derive the analytical expressions of the theoretical conjugate cam profile and the functions of the angular motion and angular velocity between the conjugate cam and the crank. Subsequently, the principle and case of the parametric sensitivity analysis are presented.

2. Basic design of the conjugate cam-spatial link feeding mechanisms

In the conjugate cam-spatial link feeding mechanisms, the driving power originates from the conjugate camshaft. Both cams in general are rigidly connected together, one of which is called the master cam, and the other is called the complementary cam. When the master cam is in pushing motion, the complementary cam can play a constraint role, and vice versa. Therefore, when the camshaft rotates, the roller followers mounted on the cams are forced to swing with some rules. In the meantime, the rocker, connected with the roller followers, pushes through the linkage, the auxiliary rod, and the crank pinion to perform the required cyclic swinging. The gear coaxial with the crankshaft is meshed with the rack, pushing the rack and the mechanisms on the rack to complete the feeding motions.

2.1 *Analytical expressions for the conjugate cam profiles*

The analytical expressions for both theoretic cam profiles must be derived first and were previously provided in [11], [12]. For convenient discussion, we reformulate the expressions in detail, according to the manufacturing requirements. To design the conjugate cam mechanism shown in Figure 2, several parameters, such as both arm lengths of the follower (l_{AO1}), subtending angle $\varphi = \varphi_1 + \varphi_{01}$, the distance between the cam center O and the follower pivot point O_1 (l_{OO1}), the roller radius r and base circle radius (r_{base}), must be provided. The arm length of both followers and the corresponding radius of rollers can be chosen to be equal or not. To simplify the manufacturing process, the length of both swinging links and the radii of both rollers is assumed to be equal.

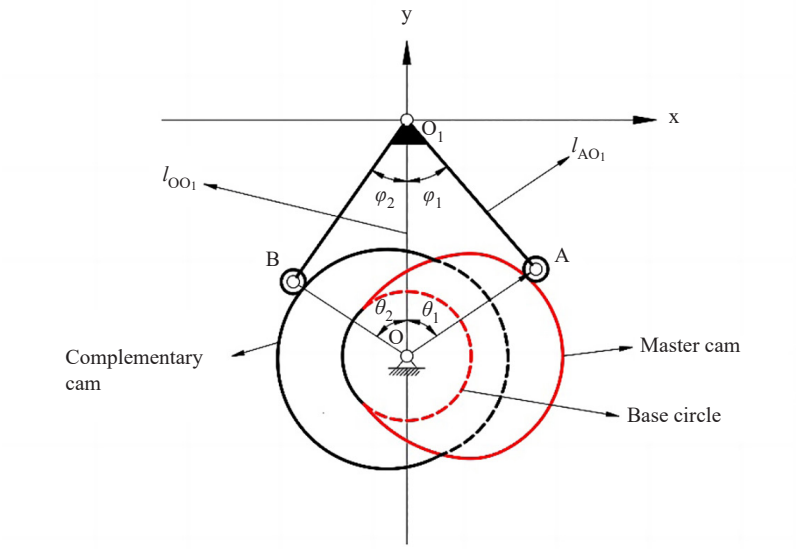

Figure 2. Schematic diagram of the conjugate cams with two roller followers

The initial angles of both swing links on the master and complementary cams can be written as

$$\varphi_{01} = \arccos((l_{OO_1}^2 + l_{AO_1}^2 - (r + r_{base})^2 / 2 l_{OO_1} l_{AO_1})$$

$$\varphi_{02} = \varphi_{total} - \varphi_{01} \tag{1}$$

The initial mounting angle on the master cam is

$$\theta_{01} = \arccos\left\{[l_{OO_1}^2 + (r + r_{base})^2 - l_{AO_1}^2]/2 l_{OO_1} (r + r_{base})\right\} \tag{2}$$

and the initial mounting angle on the complementary cam is

$$\mathrm{OB} = \sqrt{l_{AO_1}^2 + l_{OO_1}^2 - 2 l_{AO_1} l_{OO_1} \cos(\varphi_{02})}$$

$$\theta_{02} = \arccos((l_{OO_1}^2 + \mathrm{OB}^2 - l_{AO_1}^2)/2 l_{OO_1} \mathrm{OB}) \tag{3}$$

In designing the cam profiles, it is first necessary to assign the governing function (f), which can describe the relations between the follower angular motion and the conjugate cam rotation angle, namely, $\Delta\theta_1 = f(\Delta\varphi_1)$. Here $\varphi_1 = \varphi_{01} + \Delta\varphi_1$ and $\theta_1 = \theta_{01} + \Delta\theta_1$. The f frequently used involves constant speed motion, constant acceleration and deceleration motion, cosine acceleration motion, sinusoidal acceleration motion, polynomial motion, and combination motion. In the design of the conjugate cam-spatial link feeding mechanisms, the roller followers follow motions such as near-dwelling, fast-forwarding, working-feeding, slow-forwarding, far-dwelling, fast-returning, quick-feeding-back and slow-returning. Therefore, the combination motion is applied. In the fast-forwarding and slow-forwarding motions of the follower during the pushing process, cycloidal motion is applied, and polynomial motion is adopted when the followers follow the work forwarding. For simplification, the first-order polynomial is used in the design. Similarly, for

both fast-returning and slow-returning during the returning process, the same cycloidal motion is used, and the first-order polynomial is performed during quick feeding back. It is noted that the first- and second-order derivatives of the *f* function should be continuous at the joint between the motions to avoid rigid or flexible impacts.

It is important to assign the angle of the follower for every motion to ensure that the machining time is less than 10s at every station. The parameters at every station can be optimized by using the genetic algorithm [13]. During the pushing process for swing link O_1A, as shown in Figure 2, it is assumed that the maximum swing angle φ_{max}, the angle of the fast-forwarding φ_{f_fast}, the angle of slow-forwarding φ_{f_slow}, and the corresponding master cam rotation angle θ_{push}, θ_{f_fast}, θ_{f_slow}. To ensure the continuity and derivability of the first- and second-order functions of the *f* function, the following boundary conditions must be met.

$$\begin{cases} \theta_{f\_fast} = \dfrac{2\varphi_{f\_fast}}{\varphi_{max} + \varphi_{f\_fast} + \varphi_{f\_slow}} \theta_{push} \\ \theta_{f\_low} = \dfrac{2\varphi_{f\_low}}{\varphi_{max} + \varphi_{f\_fast} + \varphi_{f\_slow}} \theta_{push} \end{cases} \tag{4}$$

Therefore, the formulations of the angular motion, angular velocity, and angular acceleration for the swing link can be expressed as follows. It is noted that in the following expressions, the cam rotation angles do not include the near-dwelling angle, and in the practical calculation, the near-dwelling angle should be involved.

1) the fast-forwarding domain during the pushing

The expression of the angular motion for the swing link can be written as

$$\Delta\varphi_{f\_fast} = \varphi_{f\_fast}\left[\frac{\theta}{\theta_{f\_fast}} - \frac{1}{\pi}\sin\left(\frac{\pi}{\theta_{f\_fast}}\theta\right)\right] \tag{5}$$

where the parameter Φ represents the cam rotation angle. The angular velocity is:

$$\omega_{f\_fast} = \frac{d\Delta\varphi_{f\_fast}}{dt} = \frac{\omega\varphi_{f\_fast}}{\theta_{f\_fast}}\left[1 - \cos\left(\frac{\pi}{\theta_{f\_fast}}\theta\right)\right] \tag{6}$$

where ω is the cam angular velocity. The angular acceleration is:

$$\alpha_{f\_fast} = \frac{d\omega_{f\_fast}}{dt} = \frac{\pi\omega^2\varphi_{f\_fast}}{\theta_{f\_fast}^2}\sin\left(\frac{\pi}{\theta_{f\_fast}}\theta\right) \tag{7}$$

For Eq. (5)-Eq. (7), $\theta \in [0, \theta_{f\_fast}]$.

2) the slow-forwarding domain during pushing

The angular motion is given by

$$\Delta\varphi_{f\_slow} = \varphi_{max} - \frac{\varphi_{f\_slow}(\theta_{push} - \theta)}{\theta_{f\_slow}} + \frac{\varphi_{f\_slow}}{\pi}\sin\left[\frac{\pi}{\theta_{f\_slow}}(\theta_{push} - \theta)\right] \tag{8}$$

The angular velocity is given by

$$\omega_{\text{f\_slow}} = \frac{d\Delta\varphi_{\text{f\_slow}}}{dt} = \frac{\omega\varphi_{\text{f\_slow}}}{\theta_{\text{f\_slow}}} - \frac{\omega\varphi_{\text{f\_slow}}}{\theta_{\text{f\_slow}}}\cos[\frac{\pi}{\theta_{\text{f\_slow}}}(\theta_{\text{push}} - \theta)] \tag{9}$$

Then, the angular acceleration can be expressed by

$$\alpha_{\text{f\_slow}} = \frac{d\omega_{\text{f\_slow}}}{dt} = -\frac{\pi\omega^2\varphi_{\text{f\_slow}}}{\theta^2_{\text{f\_slow}}}\sin[\frac{\pi}{\theta_{\text{f\_slow}}}(\theta_{\text{push}} - \theta)] \tag{10}$$

For Eq. (8)-Eq. (10), $\theta \in [\theta_{\text{push}} - \theta_{\text{f\_low}}, \theta_{\text{push}}]$.

3) the working-feeding domain during pushing

The angular motion for the swing link is given as:

$$\Delta\varphi_{\text{f\_work}} = \varphi_{\text{f\_fast}} + \frac{\varphi_{\max} - \varphi_{\text{f\_slow}} - \varphi_{\text{slow}}}{\theta_{\text{push}} - \theta_{\text{f\_slow}} - \theta_{\text{f\_fast}}}(\theta - \theta_{\text{f\_fast}}) \tag{11}$$

Accordingly, the angular velocity for the swing link is given by

$$\omega_{\text{f\_work}} = \frac{d\Delta\varphi_{\text{f\_work}}}{dt} = \frac{\varphi_{\max} - \varphi_{\text{f\_slow}} - \varphi_{\text{slow}}}{\theta_{\text{push}} - \theta_{\text{f\_slow}} - \theta_{\text{f\_fast}}} \tag{12}$$

The angular velocity of the working feeding for the swing link is a constant, which thus results in zero acceleration, that is,

$$\alpha_{\text{f\_work}} = \frac{d\omega_{\text{f\_work}}}{dt} = 0 \tag{13}$$

For Eq. (11)-Eq. (12), $\theta \in [\theta_{\text{f\_fast}}, \theta_{\text{push}} - \theta_{\text{f\_low}}]$.

The feeding motions of the multi-station machine tool can be performed by the transferring units, such as the swing link, rocker, linkage, auxiliary rod, and crank. There generally exists a pause for the feeding mechanisms at the end of the working-feeding motion, which corresponds to the conjugate cam far-dwelling. Similar to pushing, the retreat of the conjugate cam also involves three parts: fast return, quick feeding back, and slow return. During the retreat, the following boundary conditions should also be satisfied, as indicated in Eq. (14). It is assumed that the angle of the swing link for fast return is $\varphi_{\text{r\_fast}}$, the corresponding conjugate cam rotation angle $\theta_{\text{r-fast}}$, and the slow return $\varphi_{\text{r\_fast}}$, the corresponding conjugate cam rotation angle $\theta_{\text{r-slow}}$. The maximum swing angle for pushing is equal to that for returning, and the corresponding conjugate cam rotation is θ_{return}.

$$\begin{cases} \theta_{\text{r\_fast}} = \dfrac{2\varphi_{\text{r\_fast}}}{\varphi_{\max} + \varphi_{\text{r\_fast}} + \varphi_{\text{r\_slow}}}\theta_{\text{return}} \\ \theta_{\text{r\_slow}} = \dfrac{2\varphi_{\text{r\_low}}}{\varphi_{\max} + \varphi_{\text{r\_fast}} + \varphi_{\text{r\_slow}}}\theta_{\text{return}} \end{cases} \tag{14}$$

Therefore, the relation between the cam rotation angle and the swing angle can be described as follows during returning (the angles for the near-dwelling, far-dwelling, and pushing are not involved).

1) the fast-returning domain during the returning
The equation of the angular motion for the swing bar is as follows:

$$\Delta\varphi_{\text{r\_fast}} = \varphi_{\max} - \varphi_{\text{r\_fast}}[\frac{\theta}{\theta_{\text{r\_fast}}} - \frac{1}{\pi}\sin(\frac{\pi}{\theta_{\text{r\_fast}}}\theta)] \tag{15}$$

thus, the expression of the angular velocity will be:

$$\omega_{\text{r\_fast}} = \frac{d\Delta\varphi_{\text{r\_fast}}}{dt} = -\frac{\omega\varphi_{\text{r\_fast}}}{\theta_{\text{r\_fast}}}[1-\cos(\frac{\pi}{\theta_{\text{r\_fast}}}\theta)] \tag{16}$$

Both the angular motion and the angular velocity lead to the angular acceleration being:

$$a_{\text{r\_fast}} = \frac{d\omega_{\text{r\_fast}}}{dt} = -\frac{\pi\omega^2\varphi_{\text{r\_fast}}}{\theta^2_{\text{r\_fast}}}\sin(\frac{\pi}{\theta_{\text{r\_fast}}}\theta) \tag{17}$$

For Eq. (15)-Eq. (17), $\theta \in [0, \theta_{\text{r\_fast}}]$.
2) the slow-returning domain during the returning
The angular motion for the swing bar is:

$$\Delta\varphi_{\text{r\_slow}} = \frac{\varphi_{\text{r\_slow}}(\theta_{\text{return}}-\theta)}{\theta_{\text{r\_slow}}} - \frac{\varphi_{\text{r\_slow}}}{\pi}\sin[\frac{\pi}{\theta_{\text{r\_slow}}}(\theta_{\text{return}}-\theta)] \tag{18}$$

Thus, the angular velocity, the derivation of the angular motion with respect to time, is obtained

$$\omega_{\text{r\_slow}} = \frac{d\Delta\varphi_{\text{r\_slow}}}{dt} = -\frac{\varphi_{\text{r\_slow}}\omega}{\theta_{\text{r\_slow}}}\{1-\cos[\frac{\pi}{\theta_{\text{r\_slow}}}(\theta_{\text{return}}-\theta)]\} \tag{19}$$

Furthermore, the angular acceleration can be obtained by differentiating the angular velocity with respect to time:

$$a_{\text{r\_slow}} = \frac{d\omega_{\text{r\_slow}}}{dt} = \frac{\pi\omega^2\varphi_{\text{r\_slow}}}{\theta^2_{\text{r\_slow}}}\sin[\frac{\pi}{\theta_{\text{r\_slow}}}(\theta_{\text{return}}-\theta)] \tag{20}$$

For Eq. (18)-Eq. (20), $\theta \in [\theta_{\text{return}} - \theta_{\text{r\_low}}, \theta_{\text{return}}]$.
3) the quick-feeding-back domain during the returning
The angular motion for the quick-feeding-back is:

$$\Delta\varphi_{\text{r\_retreat}} = \varphi_{\max} - \varphi_{\text{r\_fast}} - \frac{\varphi_{\max}-\varphi_{\text{r\_fast}}-\varphi_{\text{r\_slow}}}{\theta_{\text{return}}-\theta_{\text{r\_fast}}-\theta_{\text{r\_slow}}}(\theta-\theta_{\text{return}}) \tag{21}$$

We then have the angular velocity

$$\omega_{\text{r\_retreat}} = \frac{d\Delta\varphi_{\text{r\_work}}}{dt} = \frac{\varphi_{\max} - \varphi_{\text{r\_fast}} - \varphi_{\text{r\_slow}}}{\theta_{\text{return}} - \theta_{\text{r\_fast}} - \theta_{\text{r\_slow}}}\omega \tag{22}$$

and the below angular acceleration

$$\alpha_{\text{r\_retreat}} = \frac{d\omega_{\text{r\_retreat}}}{dt} = 0 \tag{23}$$

For Eq. (21)-Eq. (22), $\theta \in [\theta_{\text{return}} - \theta_{\text{r\_fast}}, \theta_{\text{return}} - \theta_{\text{r\_low}}]$.

To date, the problems, with respect to the function of the cam angle and angular motion, angular velocity, and angular acceleration for the swing link, are reformulated, which may be the most important in the design of the cam profiles.

For the conjugate cams, as shown in Figure 2, the coordinates of both A and B points are:

$$\begin{aligned} x_{\text{A}} &= l_{\text{AO}_1}\sin(\varphi_1) \\ y_{\text{A}} &= -l_{\text{AO}_1}\cos(\varphi_1) \\ x_{\text{B}} &= l_{\text{AO}_1}\sin(\pi/2 + \varphi_2 + \Delta\varphi) \\ y_{\text{B}} &= -l_{\text{AO}_1}\cos(\pi/2 + \varphi_2 + \Delta\varphi) \end{aligned} \tag{24}$$

where the $\Delta\varphi$ represents the swing angle. The value is positive when the conjugate cam is pushing and negative otherwise. Therefore, the theoretical profiles of the master and complementary cams can be obtained in terms of the radius vector at the different cam rotation angles, which can be expressed as

$$\begin{aligned} \overrightarrow{R_{\text{A}}} &= \sqrt{[0 - l_{\text{AO}_1}\sin(\varphi_1)]^2 + [-l_{\text{OO}_1} + l_{\text{AO}_1}\cos(\varphi_1)]^2} \\ \overrightarrow{R_{\text{B}}} &= \sqrt{[0 - l_{\text{AO}_1}\sin(\pi/2 + \varphi_2 + \Delta\varphi)]^2 + [-l_{\text{OO}_1} + \cos(\pi/2 + \varphi_2 + \Delta\varphi)]^2} \end{aligned} \tag{25}$$

The curves determined by Eq. (25), are the paths of the center of the roller, instead of the profiles of the conjugate cams. The practical profiles enveloped by the trajectory of the roller can be obtained by normally inwardly offsetting a distance of the follower roller. It is noted that the curvature radii of any point of the profiles should be 3 mm-5 mm larger than that of the roller [14] to avoid excessive contact stress [15] and transferring distortion.

For examining Eq. (4)-Eq. (23), we compute the angular motion, the angular velocity, and the angular acceleration of the followers with respect to the cam rotation angle for a specific case. For a convenient comparison, the three curves are presented in one plot, as shown in Figure 3. It is clear that the follower curves of the angular motion, the angular velocity, and the angular acceleration are smooth and continuous at any conjugate cam rotation angle, which verifies the conjugate cam profile validities as an actuating way. In addition, the followers experience near-dwelling, fast-forwarding, working-feeding, slow-forwarding, far-dwelling, fast-returning, quick-feeding-back, and slow-returning, which is necessary for the feeding mechanisms. Therefore, the selected follower motion functions and the set boundary conditions are appropriate for designing the conjugate cam-spatial linkage feeding mechanisms for the multi-station assembled machine.

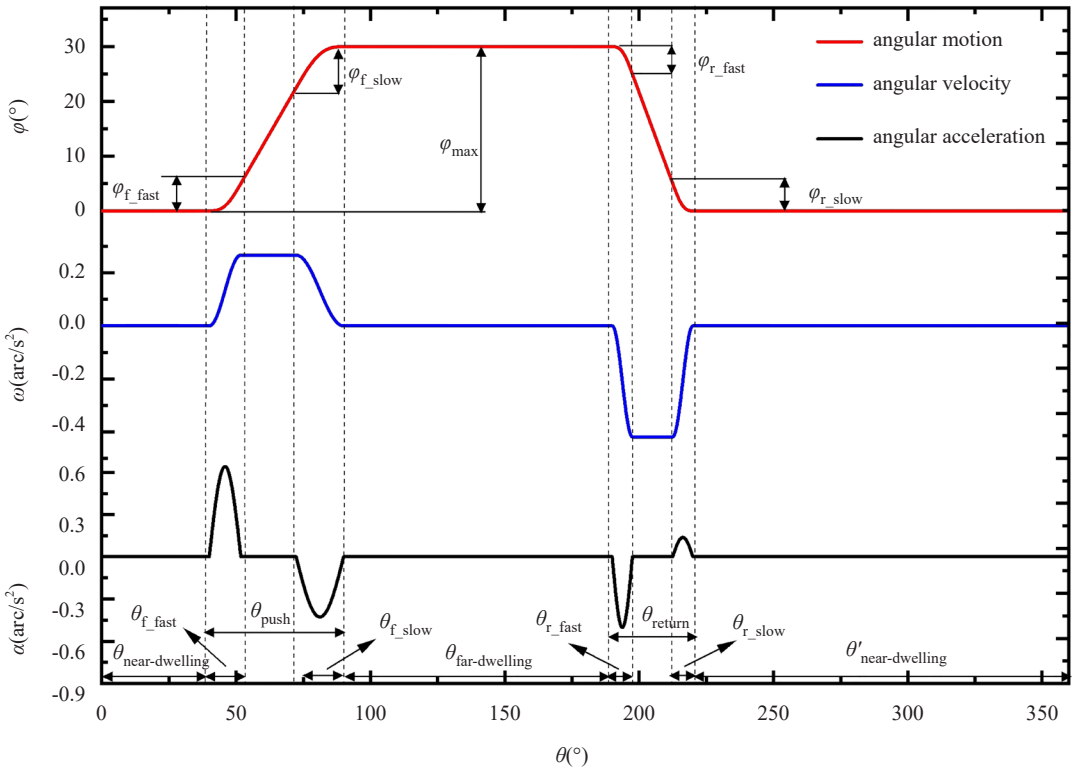

Figure 3. The theoretical angular motion, velocity, and acceleration with respect to the cam rotation angle

2.2 *Analytical expressions for the angular motion between the rocker and the crank*

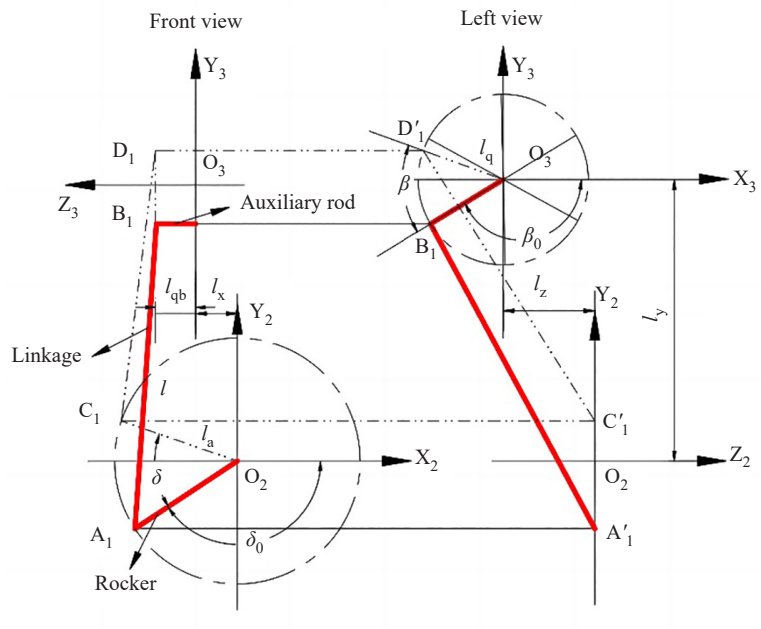

Figure 4. The schematic diagram of the rocker-crank mechanisms

The oscillations of the follower following the conjugate cam rotations are presented above. To determine the motion relations between the crank and the rocker, by simplifying Figure 1, a schematic model is built, as shown in Figure 4. In the model, two Cartesian coordinate systems ($X_2O_2Y_2$ and $X_3O_3Y_3$) fixed on the rocker and auxiliary rod are set up, in which the positive directions of the Z_2 and Z_3 axes are outwardly pointed to the faces of the rocker and auxiliary rod and with the origins at the fixed center pivot O_2 and O_3. The positive directions of the Y_2 and Y_3 axes are vertical. Therefore, the direction of the X axis is determined by the directions of the Y and Z axes, according to the right-hand rule of the spatial rectangular coordinate system. The Cartesian coordinate system $X_3O_3Y_3$ offsets the distances l_x, l_y, and l_z with respect to $X_2O_2Y_2$ and rotates around Y_2 by $3\pi/2$. Therefore, in $X_2O_2Y_2$, the coordinates of the A_1 and C_1 points are, respectively $(X_{2A1}, Y_{2A1}, Z_{2A1}) = (l_a\cos(\delta_0), l_a\sin(\delta_0),0)$, $(X_{2C1}, Y_{2C1}, Z_{2C1}) = (l_a\cos(\delta_0 + \delta), l_a\sin(\delta_0 + \delta), 0)$. Similarly, we can compute the coordinates of the B_1 and D_1 points in $X_3O_3Y_3$ as $(X_{3B1}, Y_{3B1}, Z_{3B1}) = (l_q\cos(\beta_0), l_q\sin(\beta_0),l_{qb})$, $(X_{3D1}, Y_{3D1}, Z_{3D1}) = (l_q\cos(\beta_0 + \beta), l_q\sin(\beta_0 + \beta), l_{qb})$.

To obtain the function between the parameter δ and the parameter β, it is necessary to derive the coordinates of both B_1 and D_1 points in $X_2O_2Y_2$. The coordinates of both B_1 and D_1 points can be expressed in another way by using the homogeneous coordinate transform method:

$$(x_{2B1}, y_{2B1}, z_{2B1}) = T(x_{3B1}, y_{3B1}, z_{3B1})$$

$$(x_{2D1}, y_{2D1}, z_{2D1}) = T(x_{3D1}, y_{3D1}, z_{3D1}) \tag{26}$$

where T is the matrix of the homogeneous coordinate transform. As mentioned above, $X_3O_3Y_3$ is offset along three directions of $X_2O_2Y_2$ and rotated around Y_2 by $3\pi/2$, thus,

$$T = \begin{bmatrix} 1 & 0 & 0 & l_x \\ 0 & 1 & 0 & l_y \\ 0 & 0 & 0 & l_z \\ 0 & 0 & 0 & 1 \end{bmatrix} \begin{bmatrix} \cos(\frac{3\pi}{2}) & 0 & \sin(\frac{3\pi}{2}) & 0 \\ 0 & 1 & 0 & 0 \\ -\sin(\frac{3\pi}{2}) & 0 & \cos(\frac{3\pi}{2}) & 0 \\ 0 & 0 & 0 & 1 \end{bmatrix} = \begin{bmatrix} 0 & 0 & -1 & l_x \\ 0 & 1 & 0 & l_y \\ 1 & 0 & 0 & l_z \\ 0 & 0 & 0 & 1 \end{bmatrix} \tag{27}$$

As a result, the coordinates of the B_1 and D_1 points are the following in $X_2O_2Y_2$:

$$(x_{2B1}, y_{2B1}, z_{2B1}) = (-z_{3B1} + l_x, y_{3B1} + l_y, x_{3B1} + l_z)$$

$$(x_{2D1}, y_{2D1}, z_{2D1}) = (-z_{3D1} + l_x, y_{3D1} + l_y, x_{3D1} + l_z) \tag{28}$$

The length of linkage A_1B_1 (l), as a constant, can be expressed as

$$l = \sqrt{(x_{A1} - x_{B1})^2 + (y_{A1} - y_{B1})^2 + (z_{A1} - z_{B1})^2}$$

$$= \sqrt{(l_a\cos(\delta_0) - l_x + l_{qb})^2 + (l_a\sin(\delta_0) - l_q\sin(\beta_0) - l_y)^2 + (l_q\cos(\beta_0) + l_z)^2} \tag{29}$$

Obviously, the length of A_1B_1 is equal to that of C_1D_1.

Let

$$s_1 = l^2 - (l_a \cos(\delta_0 + \delta) - l_x + l_{qb})^2$$

$$s_2 = l_a \sin(\delta_0 + \delta) - l_y$$

$$s_3 = {s_2}^2 + {l_q}^2 + {l_z}^2 - s_1$$

$$s_4 = \frac{-s_3}{2 l_q l_z},\ s_5 = \frac{s_2}{l_z}$$

$$s_6 = \frac{2 s_4 s_5}{1 + {s_5}^2},\ s_7 = \frac{{s_4}^2 - 1}{1 + {s_5}^2} \tag{30}$$

Finally, we can obtain

$$\sin(\beta_0 + \beta) = \frac{-s_6 \pm \sqrt{{s_6}^2 - 4 s_7}}{2} \tag{31}$$

According to the initial conditions, $\delta = 0$, then $\beta = 0$. Thus, the final expression for δ and β is

$$\beta = -\beta_0 + \arcsin\left(\frac{-s_6 - \sqrt{{s_6}^2 - 4 s_7}}{2}\right) \tag{32}$$

2.3 *Analytical expressions for the angular velocity between the rocker and the crank*

The feeding time is required to be less than 10s in the multi-station assembled machine at every work cycle, so it is necessary to deduce the angular velocity between the conjugate cam and the crank. As stated above, the conjugate cam angular velocity is ω, and the follower angular velocity is ω_{AO1}. The crank angular velocity will be:

$$\omega_{qubin} = \frac{d\beta}{dt} = \frac{d[\arcsin(\frac{-s_6 - \sqrt{{s_6}^2 - 4 s_7}}{2})]}{dt} \tag{33}$$

The angular velocity function between the conjugate cam and the crank can be obtained by substituting Eq. (30) into Eq. (33).

3. Case and analysis

We have provided the oscillation parameters of the roller follower, such as the angular motion, the angular velocity, and the angular acceleration, following the conjugate cam rotation and further deduced the motion function relations between the crank and the conjugate cam. In practice, we completed the design of the conjugate cam-spatial linkage feeding mechanisms of the multi-station assembled machine by reasonably assigning the component values, such as the

arm lengths of the follower, lengths of the rocker, and linkage, after carefully analyzing the machining requirements of the part. To verify the mechanism motion validation, one case is presented in the following (the parameters in Table 1 and Table 2 provided here are not those in the practical design).

Table 1. Length values in the following calculation (mm)

l_{AO1}	l_{OO1}	r	r_{base}	l_x	l_y	l_z	l_{qb}	l_a	l_q
80	160	20	50	-100	900	-150	200	220	150

Table 2. Angular values in the following calculation (degree)

φ_{total}	α_0	β_0	θ_{near}	φ_{max}	θ_{push}	φ_{f_fast}	φ_{f_slow}	θ_{far}	φ_{r_fast}	φ_{r_slow}	θ_{return}	θ'_{near}
100	-160	-150	40	30	50	5	7.5	100	5	5	30	140

The angular motion and angular velocity of the master follower and crank are shown in Figure 5(a) and Figure 5(b), respectively. It is seen that the power of the conjugate cam can be transferred to the crank using the conjugate cam-spatial linkage mechanisms, and the feeding motion will be accomplished by the mesh of the rack and pinion coaxial to the crank. Figure 5 also indicates that the angular motion and the angular velocity of the crank, except the near-dwelling crank, are always greater than those of the follower. This is attributed to the fact that the arm length of the follower is shorter than that of the rocker. In fact, the lever mechanism plays a role in amplifying the motion of the follower. In addition, as shown in Figure 5(b), it can also be seen that in the working-feeding domain, the angular velocity of the crank is not uniform, but the variable speed, after passing through the spatial linkage mechanisms, even if the follower oscillates at a constant speed. This is attributed to the nonlinear transferring characteristic of the linkage mechanisms. The nonlinear transferring characteristic of linkage mechanisms, in practical engineering design, is often used to improve working efficiency. Taking the crank shaper as an example, by using the quick return stroke of the linkage mechanisms, the moving speed of the planar tool in the noncutting stroke is far greater than that in the cutting feeding, which then results in a reduction in the nonworking time.

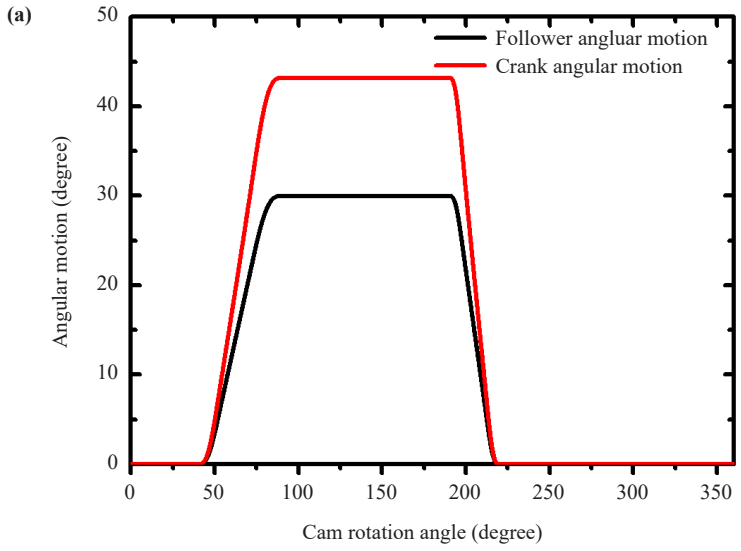

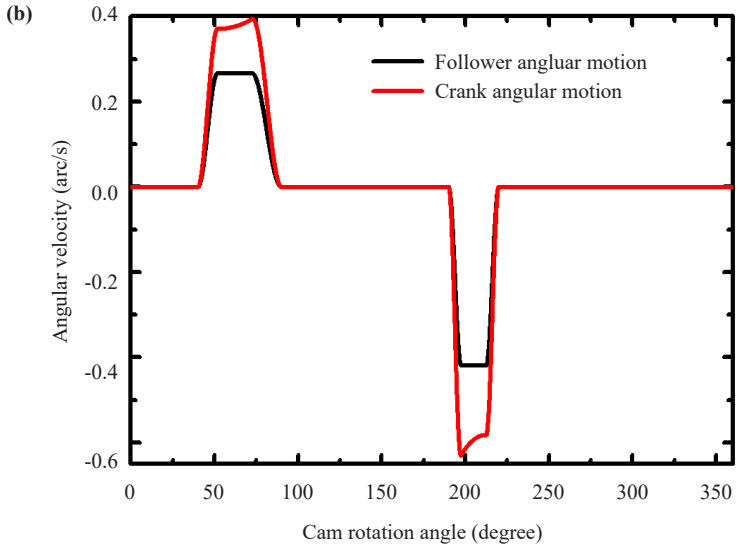

Figure 5. The angular motion and angular velocity of the follower and the crank following the cam rotation

However, the inhomogeneity of the working-feeding speed will influence the surface quality of the machined parts, thus, it is not desirable theoretically to choose the first-order polynomial function as the governing equation of the follower in the working-feeding stage. To maintain the uniformity of the working-feeding speed, assuming ω_{qubin} for the working-feeding speed to be a constant, using Eq. (29)-Eq. (33), an inverse function, that is, $\delta = g(\beta)$, is derived. The order of the higher degree polynomial is then obtained, which can be used to compute the conjugate cam profiles. In practical machining, the effect of the small inhomogeneity of the working-feeding speed on the surface quality of the machined parts can be negligible due to the higher speed of the master motion of the cutter.

Due to the errors introduced by machining and assembly, even if the mechanism is perfect in theory, noise, vibration and impact still exist. For example, the rollers connected with the swing link should always be contacted with the conjugate cams. However, because of the subtending angle errors in manufacturing or assembly, there is a gap between the roller and conjugate cam, which can lead to noise, vibration, and impact during changes in speed or direction and ultimately cause failure [16]. Therefore, it is important to analyze the influence of size errors on the transfer unit. In the design of the conjugate cam-spatial linkage feeding mechanisms, more than 20 variable parameters are involved, and furthermore, these parameters have different effects on the transferring accuracy and directions. For example, the auxiliary rod l_{qb} can influence the transferring efficiency but not the motion accuracy. On the other hand, the parameter l_{a} can affect both the transferring efficiency and the motion accuracy. Therefore, we introduce a parameter, called parametric sensitivity, to evaluate the effect of each parameter on the result.

$$S = \frac{\partial ln(X)}{\partial ln(Y)} \tag{34}$$

where X is a parameter to be evaluated, such as l_{a} and l_{q}. Y represents the parameter of the crank to be evaluated, including angular motion, angular velocity, and angular acceleration.

As an example, we calculate the angular motion and angular velocity sensitivity of the crank for both l_{a} and l_{q}, as shown in Figure 6. Figure 6 shows that both the angular motion and the angular velocity sensitivities of the crank have different tendencies. The angular motion and angular velocity sensitivities for the rocker length l_{a} are always positive, which indicates that the parameter l_{a} has a positive correlation with the angular motion and angular velocity of the crank. In addition, we can also see that the angular velocity of the crank is more sensitive than the angular motion for the parameter l_{a}; in other words, a small change in the parameter l_{a} can cause a much greater change in the angular

velocity than it does in angular motion.

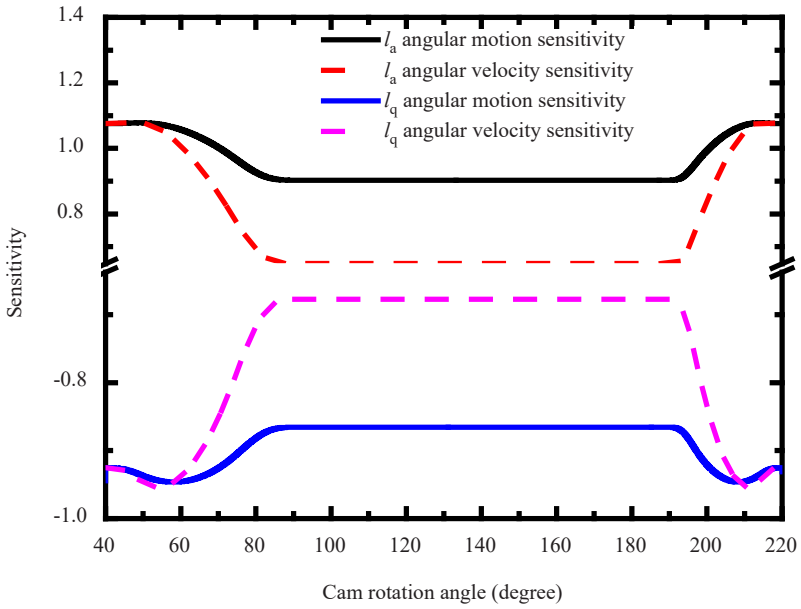

Figure 6. The sensitivity of angular motion and angular velocity of the crank for the parameters l_a, l_q

On the other hand, the parameter l_q has a negative correlation with the angular motion and angular velocity of the crank, and the sensitivity varies with respect to the cam rotation angle. Contrary to the sensitivity for the parameter l_a, the sensitivity curve for the parameter l_q rises during the forwarding process and falls during the returning process. Taking advantage of the sensitivity feature, even if there exist some size errors in l_a and l_q in the manufacturing or assembly process, the introduced errors of the angular motion and the angular velocity of the crank can be further decreased by carefully adjusting the upper and lower deviations of both parameters in the design. Similar to the analysis above, in practical design, other parameter sensitivities with respect to the angular motion and angular velocity of the crank are also analyzed to determine the upper and lower deviations.

4. Conclusion

Size errors are ubiquitous during manufacturing or assembly. Reducing or eliminating the effects of the size error on the actuator motion in complex mechanisms is a focus for mechanical designers. In this paper, a model, called parametric sensitivity, is proposed to assess the effect of the size errors on the calculated results by designing a conjugate cam-spatial linkage. By calculating the parametric sensitivity of both parameters, it can be seen that different size errors have different influences on the actuator motion. With the model, the magnitude and direction of tolerance can be determined, which makes the practical motion remain robust, even if there were some size errors of the component by carefully adjusting the tolerance of the part. The model provides a reliable basis for the size errors for the complex mechanisms.

Conflict of interest

The authors declare no competing financial interest.

References

[1] Z. H. Geng, and B. Bidanda, "Tolerance estimation and metrology for reverse engineering based remanufacturing systems", *International Journal of Production Resource*, vol. 60, no. 9, pp. 2802-2815, 2021.

[2] Z. Huang, P. X. Wei, C. Li, H. Y. Wang, and J. Y. Wang, "Aero-engine blade profile reconstruction based on adaptive step size bat algorithm and visualization of machining error", *Proceedings of the Institution of Mechanical Engineers, Part C: Journal of Mechanical Engineering Science*, vol. 234, no. 1, pp. 49-65, 2020.

[3] W.-T. Chang, and L.-I. Wu, "Calculating actual profiles of conjugate disk cams by means of conjugate variation measurement", *Journal of Mechanical Science and Technology*, vol. 25, no. 12, pp. 3083-3098, 2012.

[4] Y. Jiao, *Research on cam-linkage mechanism combination error margin to deliver and reflects shooting*. Xian, Xi'an University of Technology, 2010, pp. 6-11.

[5] J. K. Mills, L. Notash, and R. G. Fenton, "Optimal design and sensitivity analysis of flexible cam mechanisms", *Mechanism and Machine Theory*, vol. 28, no. 4, pp. 563-581, 1993.

[6] F. Djeddou, L. Smata, and H. Ferhat, "Optimization and a reliability analysis of a cam-roller follower mechanism", *Journal of Advanced Mechanical Design, System, and Manufacturing*, vol. 12, no. 7, pp. JAMDSM0121, 2018.

[7] Y. H. Yao, X. J. Wang, and H. G. Li, "Design and analysis of a high-static-low-dynamic stiffness isolator using the cam-roller-spring mechanism", *Journal of Vibration and Acoustics*, vol. 142, no. 2, pp. 021009, 2020.

[8] J. F. Hsieh, "Design and analysis of cam mechanism with negative radius roller-follower", *Transactions of the Canadian Society for Mechanical Engineering*, vol. 40, no. 1, pp. 89-100, 2016.

[9] M. Chaudhary, J. Angeles, and A. Morozov, "Design of a spherical cam-roller mechanism for an automotive differential", *Transactions of the Canadian Society for Mechanical Engineering*, vol. 40, no. 2, pp. 243-252, 2016.

[10] J. F. Hsieh, "Design and analysis of cam mechanism with translating follower having double rollers", *Transactions of the Canadian Society for Mechanical Engineering*, vol. 39, no. 3, pp. 397-406, 2015.

[11] L.-I. Wu, "Calculating conjugate cam profiles by vector equations", *Proceedings of the Institution of Mechanical Engineers, Part C: Journal of Mechanical Engineering Science*, vol. 217, no. 10, pp. 1117-1123, 2003.

[12] J. F. Hsieh, "Design and analysis of cams with three circular-arc profiles", *Mechanism and Machine Theory*, vol. 45, no. 6, pp. 955-965, 2010.

[13] L. L. Ge, L. Zhang, and K. W. Hu, "Computer aided design of conjugate cam based on genetic algorithm", *Journal Mechanical & Electrical Engineering*, vol. 38, no. 2, pp. 210-215, 2021.

[14] H. F. Du, and Y. H. Yuan, "Secondary development of the conjugated cam based on solid works. *Journal Mechanical & Electrical Engineering*, vol. 29, no. 9, pp. 1028-1031, 2012.

[15] L. S. Yousuf, and N. H. Hadi, "Contact stress distribution of a pear cam profile with roller follower mechanism", *Chinese Journal of Mechanical Engineering*, vol. 34, no. 1, pp. 1-14, 2021.

[16] P. Catala, M. A. De los Santos, J. M. Veciana, and S. Cardona, "Avoiding early failures in conjugate cam mechanism by means of different design strategies", *Journal of Mechanical Design*, vol. 138, no. 1, pp. 012302, 2016.